



McAlorum, Jack and Rubert, Tim and Fusiek, Grzegorz and Niewczas, Pawel and Zorzi, Giorgio (2018) Design and demonstration of a low-cost small-scale fatigue testing machine for multi-purpose testing of materials, sensors and structures. *Machines*, 6 (3). ISSN 2075-1702 , <http://dx.doi.org/10.3390/machines6030030>

This version is available at <https://strathprints.strath.ac.uk/64750/>

Strathprints is designed to allow users to access the research output of the University of Strathclyde. Unless otherwise explicitly stated on the manuscript, Copyright © and Moral Rights for the papers on this site are retained by the individual authors and/or other copyright owners. Please check the manuscript for details of any other licences that may have been applied. You may not engage in further distribution of the material for any profitmaking activities or any commercial gain. You may freely distribute both the url (<https://strathprints.strath.ac.uk/>) and the content of this paper for research or private study, educational, or not-for-profit purposes without prior permission or charge.

Any correspondence concerning this service should be sent to the Strathprints administrator: strathprints@strath.ac.uk

Article

Design and Demonstration of a Low-Cost Small-Scale Fatigue Testing Machine for Multi-Purpose Testing of Materials, Sensors and Structures

Jack McAlorum ^{1,*}, Tim Rubert ^{2,†}, Grzegorz Fusiek ¹, Pawel Niewczas ¹ and Giorgio Zorzi ²

¹ Department of Electronic & Electrical Engineering, University of Strathclyde, Glasgow G1 1XQ, UK; g.fusiek@strath.ac.uk (G.F.); p.niewczas@strath.ac.uk (P.N.)

² Doctoral Training Centre in Wind and Marine Energy Systems, University of Strathclyde, Glasgow G1 1XQ, UK; tim.rubert@strath.ac.uk (T.R.); giorgio.zorzi@strath.ac.uk (G.Z.)

* Correspondence: jack.mcalorum@strath.ac.uk

† These authors contributed equally to this work.

Received: 6 June 2018; Accepted: 10 July 2018; Published: 12 July 2018



Abstract: Mechanical fatigue testing of materials, prototype structures or sensors is often required prior to the deployment of these components in industrial applications. Such fatigue tests often requires the continuous long-term use of an appropriate loading machine, which can incur significant costs when outsourcing and can limit customization options. In this work, design and implementation of a low-cost small-scale machine capable of customizable fatigue experimentation on structural beams is presented. The design is thoroughly modeled using FEM software and compared to a sample experiment, demonstrating long-term endurance of the machine. This approach to fatigue testing is then evaluated against the typical cost of outsourcing in the UK, providing evidence that, for long-term testing of at least 373 h, a custom machine is the preferred option.

Keywords: fatigue; loading machine; design; low-cost; customizable; FEM software

1. Introduction

In materials science, fatigue is defined as “a localized damage process of a component produced by cyclic loading” [1]. It can be represented as a relationship between certain stress levels repeated for a certain number cycles, with additional factors also contributing to a varying fatigue limit. These include mainly the type of material, dimensions, manufacturing defects and environmental factors. Commonly, fatigue of a component is represented by an S-N curve, an example of which is shown in Figure 1a. Particular stress values cause fatigue failure at a related number of cycles according to the curve. A typical fatigue test is run by repeatedly applying a sinusoidal stress, illustrated in Figure 1b. According to the Goodman relation, a specimen will achieve infinite life if the stress amplitude σ_a remains below the endurance limit σ_e for a mean stress $\sigma_m = 0$ (Figure 1c).

Fatigue testing of materials, sensors, and structures is a key element in the design and verification process in engineering [2–5]. With fatigue tests aiming for 10^6 – 10^7 cycles and beyond, the testing processes are time consuming. This is of course dependent on the chosen cycling frequency, which will vary depending on experimental parameters. For example, in concrete structures: “cyclic frequencies are limited by the high ranges of deflection and the necessity to avoid local heating due to friction at cracks in the concrete” [6]. Therefore, in concrete testing, a lower testing frequency is necessary, which, in turn, is more time consuming.

Access to third party fatigue testing machines is limited and can be costly. Purchasing a commercially available machine comes with initial great expense that may not amortize for a short to medium-term project, but may decrease long-term costs overall. Many commercial

machines are available on the market, with varying prices that are influenced mainly by the maximum force, speed and accuracy requirements; large force, fast speeds and high accuracy that characterize the machine are accompanied by a large cost. A third option is to design and build a machine from individual components capable of producing required load cycles. Not only will this allow full control over the capabilities of the machine, but it may decrease the total project cost significantly.

In this manuscript, the design process of a low-cost, small-scale fatigue testing machine design for multi-purpose testing of materials, sensors, and structures is exemplified. Research institutions with similar project requirements may use this type of design to reduce the overall costs of long-term fatigue cycling. The paper is structured as follows: Section 2 describes the requirements of the machine in this work, Section 3 presents a review of reported machine designs for fatigue testing purposes, whilst Section 4 describes the methodology for approaching the task. Section 5 presents comparison of potential actuators followed by Section 6 which outlines the initial computer-aided design (CAD) and finite element method (FEM) model of the support frame. Section 7 discusses the installation and commissioning procedure before the previous FEM models are compared to experimental tests in Section 8. Section 9 provides information on the commercial benefit of custom machine building to outsourcing, and the paper is concluded in Section 10.

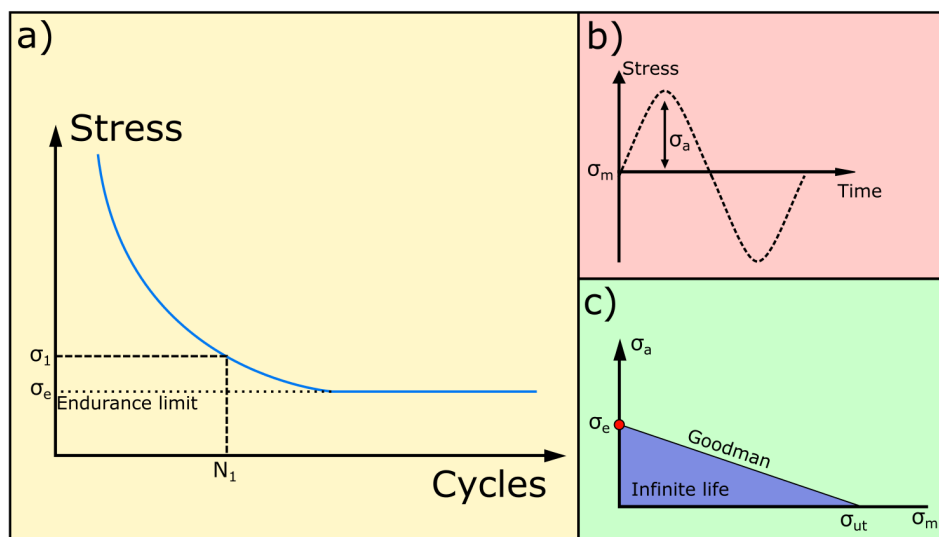


Figure 1. (a) example of an S–N curve illustrating fatigue of an arbitrary component where failure would occur for a stress of σ_1 after N_1 cycles; (b) one cycle of a typical sinusoidal fatigue test and (c) the Goodman relation. The Goodman relation states that for a stress amplitude, σ_a , less than the endurance limit, σ_e , no fatigue shall occur and infinite life should be achieved.

2. Design Requirements

2.1. Intended Experiments and Required Force

The design of a fatigue testing machine is highly dependent on the intended testing specimen. This includes geometry, material properties and experimental procedure, which will also define the necessary force. In this work, the machine will primarily be used to test concrete beams with the following maximum geometry: $1 \times 0.1 \times 0.1$ m (length \times width \times height). Values are chosen to provide adequate areas for multiple sensors to be applied to beam faces. In addition, the focus of the research for this machine is to test sensors applied to pre-cracked concrete specimens; therefore, a key requirement is the ability to both open and close these cracks. To do this, the actuator must be capable of bi-directional force application to the specimen. The stress ratio, R , defines the type of loading:

$$R = \frac{F_{min}}{F_{max}} = \frac{\sigma_{min}}{\sigma_{max}} = \frac{\epsilon_{min}}{\epsilon_{max}}, \quad (1)$$

where tension–tension, $0 < R < 1$, compression–compression $R > 1$, and bi-directional, $R < 0$. For equal magnitude, bi-directional force, $R = -1$. A machine capable of all ratios will allow a more thorough fatigue testing capability and a more flexible machine overall.

The standard practice for fatigue testing is the application of a sinusoidal waveform; however, loading during real-world applications is rarely absolute [7]. The British standards [8] suggest “When assessing fatigue performance, a realistic estimate of the fatigue loading is crucial to the calculation of life, and all types of cyclic loading should be taken into account”. Therefore, a customizable force application to produce either sinusoidal or other shaped waveform with variable amplitude and frequency is required.

Machine geometry requires adjustment depending on the yield point of the material in order to reach the necessary strains and stresses in the sample. The initial objective was to produce an adequate strain level for testing sensors on a concrete beam face. We can calculate the maximum strain level ϵ_{max} on the concrete beam face due to maximum force F_{max} as:

$$\epsilon_{max} = \frac{M_{max}H}{2I_s E_C}, \quad (2)$$

where maximum moment M_{Max} is given by:

$$M_{max} = \frac{2F_{max}H^4}{L^3} \quad (3)$$

for $F_{max} = +25$ kN, $M_{max} = 3125$ Nm, where $H = 0.1$ m is the height and width of the beam and $L = 1$ m is the beam length. Substituting Young’s modulus of concrete $E_C = 17$ GPa and area moment of inertia for the 0.1 m square cross section $I_s = 8.33 \times 10^{-6}$ m⁴ provides strain $\epsilon_{max} = 1.1$ mc. This strain should suffice for the intended sensor testing; therefore, aimed force is ± 25 kN.

2.2. Actuator

From Section 2.1, the required force is known to be ± 25 kN, which concentrates possible actuator choices. The following itemized list presents the optimization factors for the actuator:

- High accuracy,
- Low noise,
- High reliability,
- Long lifetime,
- Low maintenance requirements,
- Considerable customization (capable of sinusoidal load cycle),
- User friendly interface.

In addition, the variability of the stress ratio requires an adjustable control that ideally is user-friendly and software based, without any requirement to mechanically adjust the system components.

For the support frame, a few factors require consideration during design:

- Actuator and beam geometry,
- Yield stress,
- Fatigue life.

The frame must be capable of housing the actuator and beam in order to produce accurate fatigue forces (sinusoidal). However, the frame itself must be adequately designed to survive the maximum stress levels over a long period. In other words, the endurance limit, σ_e , of the frame must be greater than the expected maximum stresses during fatigue operation.

3. Review of Literature

A low-cost fatigue testing machine capable of ± 25 kN bi-directional force on a beam with dimensions: $1 \times 0.1 \times 0.1$ m (length \times width \times height) is desired as discussed previously. Reported machine designs in literature may aid in design of a custom machine and provide insight into the novelty of the work. Lee et al. [9] demonstrated the design of a structural fatigue testing machine capable of both bending and torsional loading. A hydraulic system was incorporated to both apply loading and fix the test specimen. Stress analysis of the frame is provided, with particular attention on the interface between actuator and specimen. The specified loading capability for bending is ± 490 kN and the maximum specimen size is $7500 \times 1500 \times 950$ mm. Such a machine is designed for large-scale testing, made evident by the large force. The bi-directional capability is not demonstrated during test results, so it is unclear whether this is possible. No commercial evaluation is performed and so relative cost is unknown. It is likely to be extremely costly and benefit a long-term test period. A high initial cost may not be suitable for short-medium term testing periods. Machines are regularly designed for extremely small scale fatigue testing. For example, Vincent et al. [10] and Bhatkar et al. [11] presented machines producing maximum loading in the range of 88–300 N on small specimens of length < 150 mm. The main reason for custom designs is to reduce initial costs, which is less complicated for small-scale machines. Pach et al. [12] presented a unique method for applying axial loads to specimens by using a “seesaw” motion. Although they declare a design requirement of $R < 0$ (tension-compression), this was not demonstrated due to lack of correct grip attachment. Forces were also limited to 10 kN. Costs are declared to be around \$3000 in comparison to a servohydraulic machine of \$100,000. A detailed breakdown of each section is not provided.

In terms of commercially available machines, a device capable of bi-directional loading is rare for 4-point bending applications. Cooper Technology (Ripley, UK) provides a servo-hydraulic actuator capable of bi-directional loading, but only maximum loads of ± 10 kN [13]. Instron (High Wycombe, UK) provide a few available bi-directional fatigue testing machines [14]. The electrical devices are lacking the required force; however, the hydraulic systems are more suitable, such as the 8872 servohydraulic fatigue testing system. The main issue is that the machines are not suited to beam bending and a custom frame would still be required to both load and support the beam. In some cases, the location of sourcing appropriate machines is an issue and can cause large shipping costs. Communication is also key to determining the customization possibilities of the loading cycles, which are not usually quoted.

Following the literature review, authors believe that the novelty of the work presented in this paper is as follows:

- An economic evaluation of producing a custom machine in comparison to purchasing commercially or outsourcing: which provides justification for the work.
- Capability of adjustable shape, frequency and amplitude loading cycles applied to beam specimens since real-world fatigue is rarely caused by pure sinusoidal loading.
- FEM modeling to validate the long-term testing capability of the machine—verified by experimental testing.

4. Methodology

The process in designing and commissioning the fatigue testing machine is as follows:

1. Determine the required maximum force to produce sufficient stress in predetermined test specimen. This can be exaggerated to increase specifications. For the present project, this was calculated at ± 25 kN.
2. Review and choose preferred actuator, optimizing factors outlined in Section 2.2.
3. Design suitable support frame and model in CAD software.
4. Use FEM software to ensure that support frame meets physical requirements. Model a test experiment with beam specimen.

5. Manufacture and install the machine, including electrical connections.
6. Commission the machine by programming and performing test experiments to compare to the model, validating the support frame structure.

Following these steps, the machine will be ready for further experimentation.

5. Actuator

Based on a literature review, possible actuators include pneumatics, hydraulics, and linear and servo actuators. Linear actuators are not suitable because they do not allow a variable speed application to adjust the testing frequency. With regards to pneumatic drives, machine parts are generally cheaper, require less maintenance, and are cleaner (no oil) than hydraulics [15]. However, system efficiencies are significantly worse (lower possible forces) and the system experiences a time delay. The overall anticipated issue with hydraulics and pneumatics are the necessary system complexity (associated with many valves and control switches for $R = -1$ test option), reliability and maintenance concerns as well as the emitted noise of the compressor. Ultimately, it was ascertained that a servo actuator agrees with all requirements and was thus selected as the preferred fatigue drive option.

Servo actuators are selected based on the expected total lifetime travel distance at a given applied load, thus assumptions were made with regards to the lifetime travel distance and the mean applied force. A generic example testing procedure is defined in matrix x consisting of different test cycles (1: n) with the amount of cycles C at force F , and the respective predicted distance travelled D . The travel distance may be derived from a FEM model:

$$x = \begin{bmatrix} F_1 & C_1 & D_1 \\ F_2 & C_2 & D_2 \\ F_3 & C_3 & D_3 \\ \vdots & \vdots & \vdots \\ F_n & C_n & D_n \end{bmatrix}. \quad (4)$$

With a pre-defined testing procedure, the total lifetime travel distance can be calculated by:

$$D_{tot} = \sum_{i=1}^n x_{i,2}x_{i,3}, \quad (5)$$

and the mean applied load is calculated by the cubic mean load formula (fatigue exponent of 3 [16]):

$$F_{mean} = \frac{[\sum_{i=1}^n (x_{i,1})^3 x_{i,2}x_{i,3}]^{1/3}}{D_{tot}^{1/3}}. \quad (6)$$

Depending on the cubic mean force and total travel distance assessment for the lifetime expected, the appropriate servo actuator parameters are selected. In addition, depending on the intended test cycle and force (step changes with breaks vs. continuous movements), a fan might be necessary to prevent the motor from overheating.

Due to the requirement to enable different operational modes, the servo actuator further enables user-friendly and adjustable control. The latter can be controlled by readings from a load cell that is aimed to be installed between the 4-point bending frame and the actuator and implemented through a feedback loop via the actuator controller.

6. Support Frame

Various methods can be adopted for loading a beam specimen, such as direct tension/compression, 3-point bending or cantilever. Since an objective of this work is to test sensors, it is crucial that the maximum stress position has adequate space for sensors. For this reason, 4-point bending was chosen,

as the center of the beam remains clear. This means the support frame will require fixed constraints at each end of the beam, but incorporate the capability of using a linear-single point motion from the actuator to perform 4-point bending. It is also a requirement that the beam is loaded in both directions. In other words, a single face of the beam (top or bottom) undergoes tension and compression in a single cycle. This will allow more thorough analysis and testing of the specimen and any attached sensors. With these additional requirements following the actuator choice, the frame can be designed.

6.1. CAD Model

Figure 2a shows a rendered completed frame with inserted beam and actuator, whereas Figure 2b shows an exploded isometric CAD model of the outer frame in black and the inner 4-point bending frame in red. Some key dimensions are as follows: width of frame 1.5 m, height is 1.16 m, depth is 0.254 m. The outer frame is designed to provide the necessary reactionary compression and tension forces of the linear actuator that is vertically inserted between the top two I-beams. For the outer shell, conventional sized structural steel I-beams are selected as this element enables significant tensional and compressive resistance while allowing easy sourcing without additional machining of complex parts. At each corner the I-beams are cut at an angle of 45° and in-plane full penetration butt-welded together with a steel plate in between. Welding is carried out according to British standards [17]. The top section is manufactured out of two parallel smaller I-beams in order to fit the servo actuator, while the top and bottom plates are necessary to distribute tension and compression forces onto both I-beams.

The 4-point bending frame is designed out of hollow squares, while the top two elements are made of solid pieces with threaded holes to variably attach the testing sample to enable $R < 0$ testing. The 4-point bending frame could potentially be exchanged with a simple foot to enable 3-point bending tests.

The frame is mounted onto the floor with two steel foot elements welded and an angle of 90° . The beams intended for testing are kept in place based on two bolts on the right and left that are screwed into the middle sections. These sections are attached to the side I-beams through threaded bolt attachment. Therefore, the sample can be adjusted by tightening the main bolts. Potentially greater elements may be tested; however, this would require an adjusted 4-point bending frame.

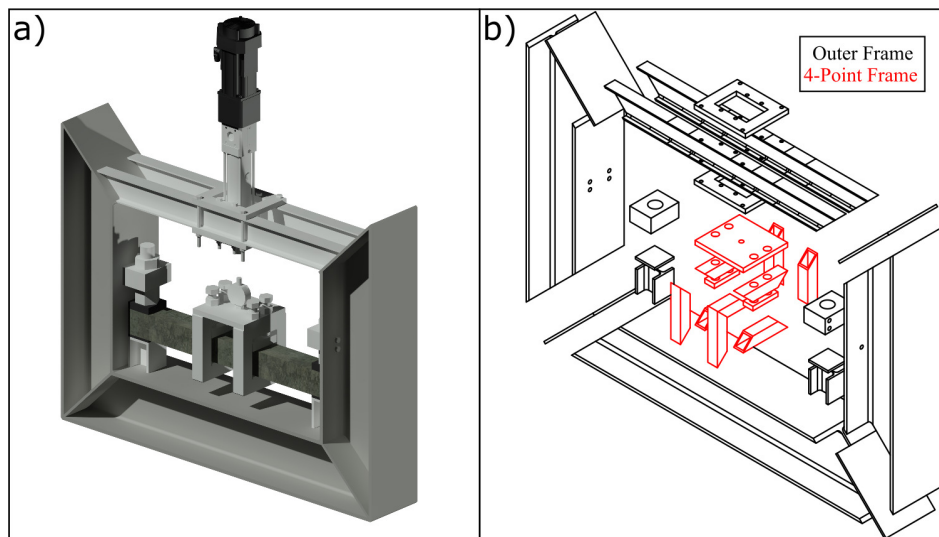


Figure 2. Isometric views of (a) rendered machine and (b) exploded frame.

6.2. FEM Model

Following the previously discussed requirements in Section 2, it is essential to ensure that stress levels in the support frame do not exceed mechanical limits during maximum loading. Fatigue life of the frame will also require consideration. The frame can mechanically be separated into two parts,

the outer and 4-point bending frame, as exemplified in Figure 2. The 4-point frame can be modeled as a singularly welded component. The outer frame consists of three separate interactions: at the actuator attachment and at the bottom and top beam supports. To simplify simulations, we will assume that this structure is also singularly welded. To reduce computational requirements, all holes and bolts will be removed—meaning real-world stress levels will differ from simulations. These simulations act as an approximate guide of the expected stress levels the frame will be subjected to.

6.2.1. Outer Frame

The geometry of the outer frame is inserted into a FEM modeling software. Figure 3 shows the stress distribution during a 25 kN load applied in five positions: upwards against the top I-beams and the two top supports as well as downwards against the two bottom supports. Any deformation is exaggerated for illustrative purposes.

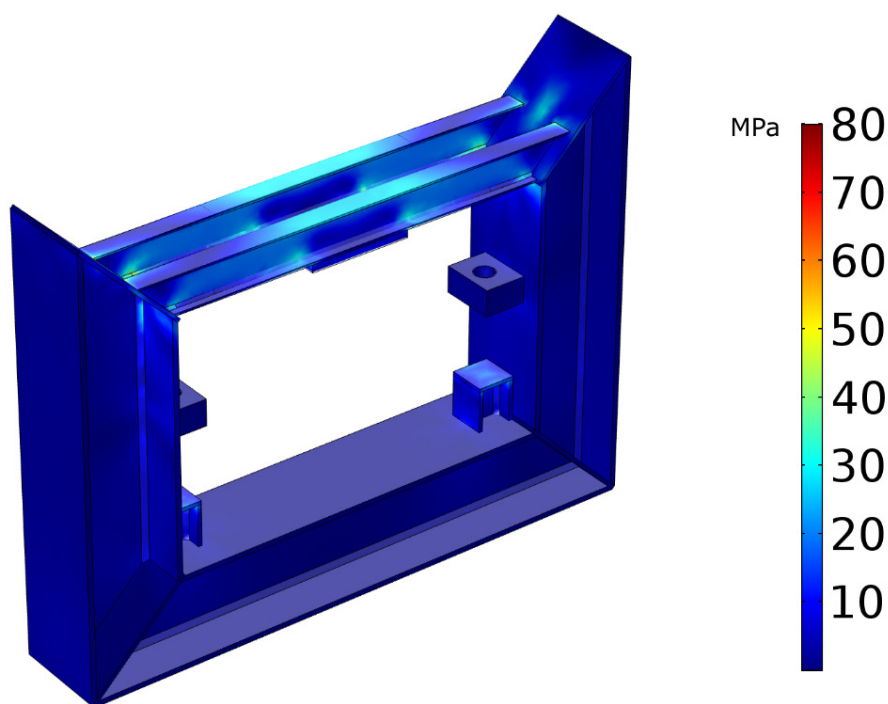


Figure 3. Stress distribution during 25 kN forces acting in all interfaces.

The scale shows the maximum stress level is 80 MPa; however, it is clear that the majority of stress in the components is below 50 MPa. This is well below both the yield stress $\sigma_y = 250$ MPa of structural steel and will also be within the endurance limit σ_e . According to Kucharczyk et al. [18], experiments on structural steel with yield limit of 430 MPa showed no endurance limit less than 260 MPa. A general approximation of $\frac{\sigma_y}{2}$ for σ_e can be used as a guideline. This means a stress of less than 125 MPa is desired to ensure long operational lifetime. We can also see that most of the stress is applied to the top I-beams. It is important to also consider the welded sections, as the endurance limit will differ to that of steel. In the case of the outer frame—the stress is focused on the attachment point of the actuator, thus welds of I-beams are not a concern. This may require more in-depth study for the 4-point frame. To acquire a more accurate value for maximum stress, we can separately model the actuator attachment point with bolt interactions. Figure 4 shows the stress distribution for the actuator attachment during a 25 kN load in the downward direction.

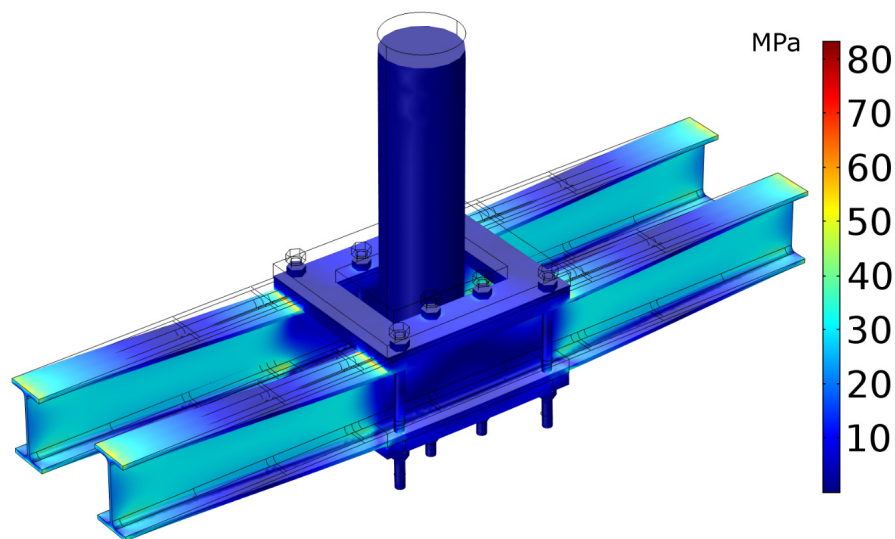


Figure 4. Stress distribution of maximum stress component: actuator attachment.

According to Figure 4, the absolute maximum stress magnitude occurs at the contact point of the actuator attachment plates to I-beams. This matches the stress limit from Figure 3. The model calculates a value of ≈ 70 MPa at this point. This is well below the estimated endurance limit of the steel, $\sigma_e = 125$ MPa. It is also possible to minimize the stress at this contact point with the introduction of a soft material, such as rubber. With stress levels in the majority of the I-beams below 40 MPa, the outer frame should survive indefinitely under continuous maximum loading conditions.

6.2.2. 4-point Frame

Following the same process, the FEM model of the 4-point frame is established by applying the maximum possible load to the bottom, shown in Figure 5.

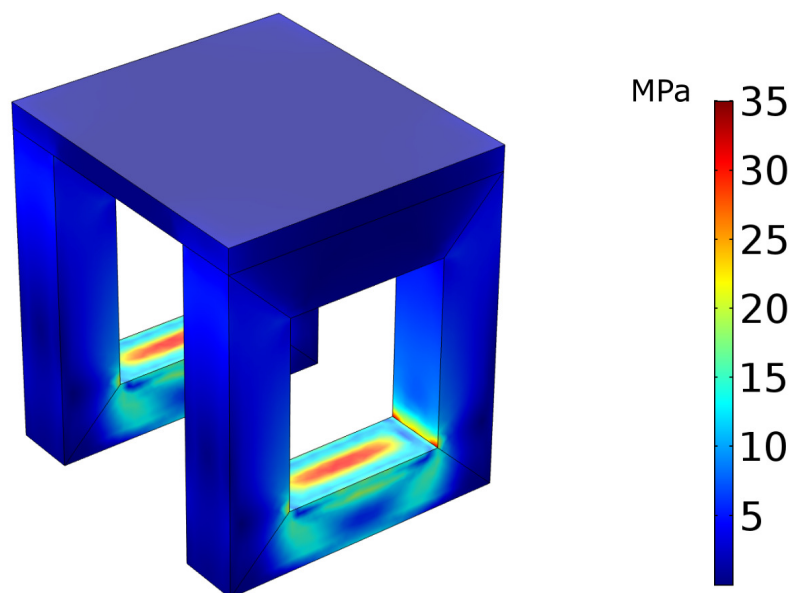


Figure 5. Stress distribution in 4-point frame during maximum loading.

Again, we see stress levels well below the approximate endurance limit, $\sigma_e = 125$ MPa. The weld interface between the hollow beams is the weakest point of this section. According to EN 1993-1-9 [19], the endurance limit for welds, σ_{ew} with detail category, $\Delta\sigma_C = 100$ can be calculated as:

$$\sigma_{ew} = 0.549 \cdot 0.737 \cdot \Delta\sigma_C, \quad (7)$$

providing a smaller endurance limit of 40.5 MPa when compared to that of steel. From Figure 5, the stress is up to 35 MPa in this region. With this information, the 4-point frame should also survive indefinitely under continuous maximum loading conditions. In the worst case scenario, according to curves shown in [19], the 4-point frame may fail after several million cycles. Since this is a significant amount of time and replacement cost would be low, this is of little concern.

6.2.3. Beam Model

As discussed in Section 2, the frame is designed to test beams of 10 cm width and height and 1 m length of any material. To validate both the force capability of the actuator and the simulations of stress levels in frame sections, it is possible to simulate and perform a single beam experiment for comparison. If strain levels witnessed in the beam during both cases are similar—this provides confidence that the frame FEM models are also accurate without the need to install more sensors. In addition, it would be highly beneficial to carry out simulations prior to any experimentation in order to determine the maximum possible strain that can be subjected to the specimen. Any new specimen can then simply be inserted into the pre-existing model and expected strains will be known prior to experimentation.

A hollow steel beam of 1 m length, 120 mm width, 60 mm height and 5 mm thick walls was chosen as a test specimen. These dimensions were firstly inserted into the FEM software, and results were shown in Figure 6.

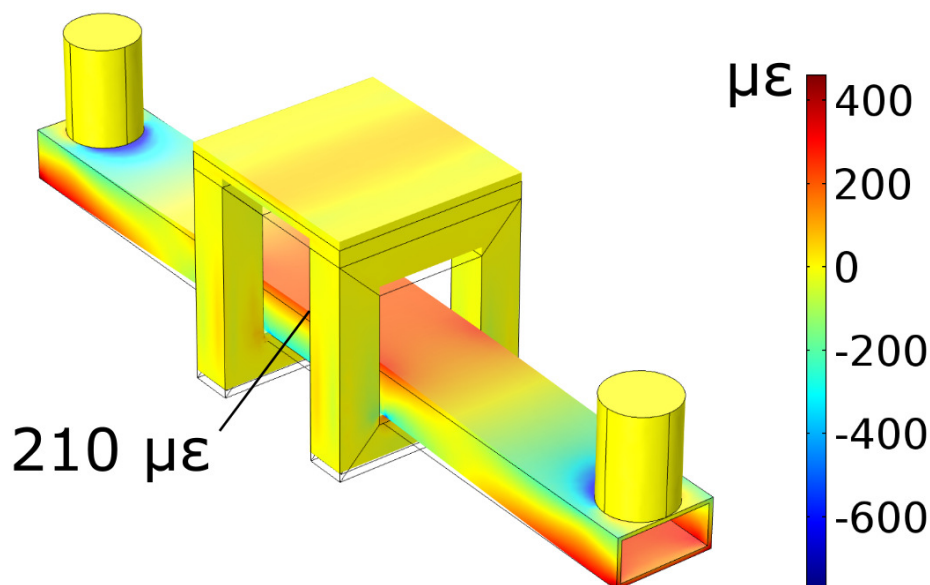


Figure 6. Stress distribution of the steel specimen.

This will be used during testing (Section 8) for comparison. A tension strain of 210 $\mu\epsilon$ was witnessed in the simulation at the mid-point of the steel specimen, as annotated.

7. Installation and Commissioning Procedure

Prior to testing, the machine requires installation and initial commissioning. This includes:

- Physical fitting of the frame, actuator, controller and PC,
- Wiring of controller, actuator, power supplies and load cell,
- Programming of actuator control software.

Following physical fitting, the electrical cabling is arranged according to Figure 7a. At this stage, the setup is simple, with extensive expandability in the form of analogue and digital inputs and outputs. In addition, 24 V DC supplies are required to power the controllers various features, such as the digital inputs/outputs, the brake and to enable the controller itself. A 400 V 3-phase supply is used for powering the motor. A feedback loop containing the amplified load cell voltage is used to determine the direction of the motor. A program is created for simple sinusoidal movement dependent on set force limits, as illustrated in Figure 7b. Three variables are set, compression force, F_1 , tension force, F_2 , and maximum speed, V_1 . During either retraction or extension, the direction of motor rotation is reversed once the set force is reached. The actuator acceleration is also customizable but was set at the default value in this work. This simple program will allow initial testing of a specimen to ensure that the machine meets design requirements.

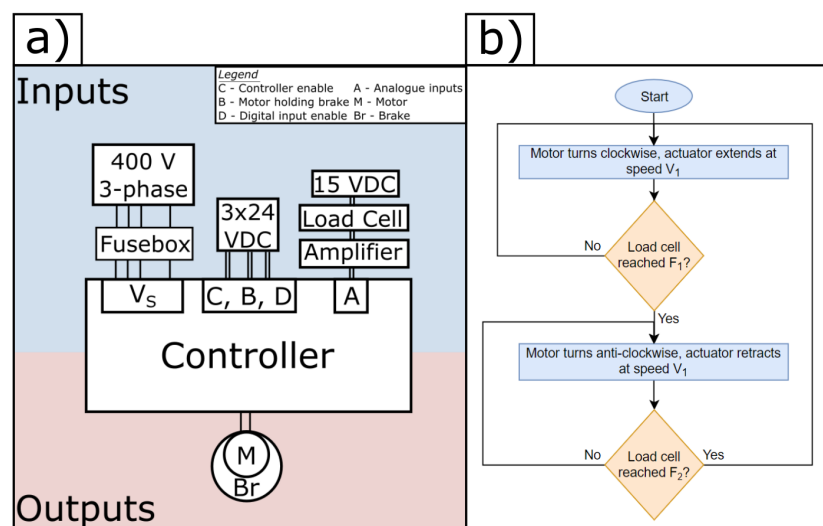


Figure 7. (a) circuit diagram of controller setup; (b) flow chart of simple load cell feedback control program. F_1 , F_2 and V_1 are force and speed values set by user.

8. Testing Results

Figure 8 shows the experimental set-up of the steel beam and frame, similar to the simulation in Figure 6. The program shown in Figure 7b was run with the force limits, F_1 and F_2 , set at ± 25 kN and an arbitrary speed. The sensor applied to the steel specimen were epoxied fibre Bragg gratings (FBGs), characterized as reported in [20]. Using the sensitivity of 0.89 nm/ $\mu\epsilon$, the strain at the centre point of the steel specimen is shown in Figure 9, with a more detailed view of the cycle inserted. The frequency of cycles is controlled by the set speed of actuator extension. Maximum linear speed of actuator is quoted as 500 mm/s. In this test, speed was set at 50 mm/s, which produced a cycle frequency of 0.5 Hz. Therefore, the maximum frequency of this load cycle is 5 Hz, although emphasis is made on the previous statement of requiring lower frequency when testing concrete. One must also consider the temperature of the controller and actuator, which may limit the cycle frequency further. An external fan is used to reduce motor temperature and was not required during the test in this work. Future work will investigate temperatures over an extended testing period. Load cell limits

can be easily adjusted, allowing variable magnitude load cycles. Load and speed variables were varied during testing to ensure successful operation over the entire range. Overall, the load cycle remains stable throughout, with a tension peak of $\approx 220 \mu\epsilon$, which, when compared to the simulation ($210 \mu\epsilon$), is in close agreement (+4.7%). The slight increase is most likely due to geometric differences of the specimen compared to the model—the corners are filleted for example. This was omitted in simulations to reduce computational requirements. It is clear that the cycles are not sinusoidal or triangular from the insert: this will be improved on by modifying the program to include a smoother transition. The accuracy of the machine can be ascertained by analysing the spread at the peaks of the load cycle. In other words, the deviation over time of the peak loading. Extracting the peak values of each individual cycle in this test provided an accuracy of $\sigma_\epsilon / \mu_\epsilon = 0.74\%$ where σ_ϵ and μ_ϵ are the standard deviation and mean of strain peaks, respectively. To compare this to similar machines is difficult as commercial machines would require significant customization to provide similar load tests. One commercial machine was used in previous work [21] for tensile loading of a steel specimen. Results from this produced an accuracy value of 1.08% that is comparable to the machine in this work. Overall, this simulation provides confidence in the previous FEM simulations, the survivability of the frame and the overall design.

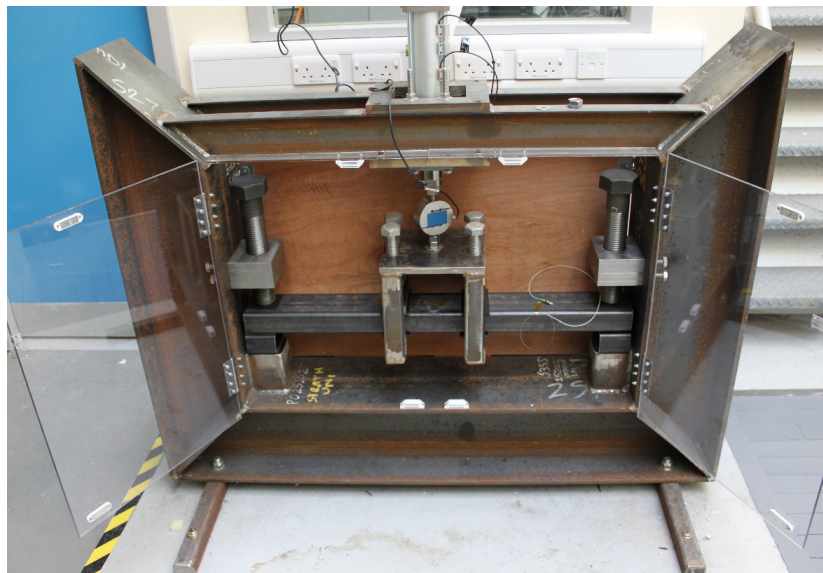


Figure 8. Experimental set-up of test specimen.

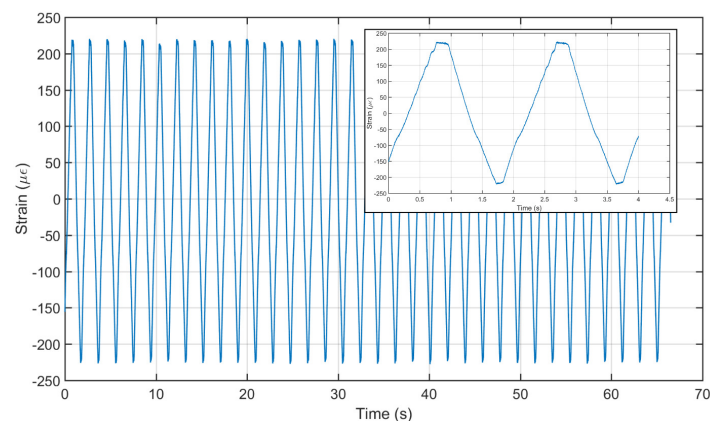


Figure 9. Strain at centre of steel beam, insert: detailed view of cycle.

9. Commercial Evaluation

Table 1 illustrates the breakdown of key components constituting the machine and their cost. Overall, the fatigue drive was the most expensive component with 59% of the overall costs. With regards to the decision-making of the insourcing of the machine (buying components and commissioning the machine) versus outsourcing of the testing, the business case depends on the intended usage.

Table 1. Machine expenditure.

Item	Cost £
Servo Actuator	12,000
Frame	5500
Equipment	2000
Installation	720
Total	20,220

Given a mean outsourcing machine expenditure of £325/day (value gained from locally available source), the cost–benefit threshold over outsourcing is reached at 373 h of testing. Assuming a sample is tested at 3 Hz, this corresponds to 4 million cycles. At 10 Hz, this corresponds to 1.34×10^7 cycles. Consequently, the lower the testing frequency, the more likely becomes the option of insourcing. As a consequence, depending on the intended total usage, the sourcing strategy may be defined.

10. Conclusions

An alternative machine design is presented for continuous long-term fatigue testing. FEM models examining stress levels in the support frame conclude that, for maximum loading, the frame should remain below the endurance limit, and thus should survive indefinitely. A steel beam specimen was also modeled and compared to real world tests, validating the previous analysis and providing an initial specimen examination for any future tests. In comparison to outsourcing, this design is cost-efficient if more than 373 h of testing is planned. The machine also provides a more customizable and less time restricted test-bench.

Author Contributions: J.M. prepared the CAD and FEM model, sourced the components, installed, commissioned and programmed the machine, and supported the overall design of the machine. T.R. generated the idea, designed and commissioned the machine, sourced the components and gave guidance with regards to the CAD and FEM. J.M. and T.R. wrote the manuscript. G.F., P.N. and G.Z. supported the work throughout.

Funding: This work was supported by ScottishPower Renewables, SSE and the Engineering and Physical Sciences Research Council, Grant No. EP/L016680/1.

Conflicts of Interest: The authors declare no conflict of interest.

Abbreviations

The following abbreviations are used in this manuscript:

CAD computer-aided design
 FEM finite element method
 FBG fibre Bragg grating

References

1. Lee, Y.L.; Pan, J.; Hathaway, R.; Barkey, M. Fatigue Damage Theories. In *Fatigue Testing and Analysis*; Elsevier: Amsterdam, The Netherlands, 2005.
2. Stephens, R.I.; Fatemi, A.; Stephens, R.R.; Fuchs, H.O. *Metal Fatigue in Engineering*; John Wiley and Sons: Hoboken, NY, USA, 2000; Volume 2.

3. Suresh, S. *Fatigue of Materials*; Cambridge University Press: Cambridge, UK, 1994.
4. Richard, H.A.; Sander, M. *Fatigue Crack Growth: Detect—Assess—Avoid*; Springer: Berlin, Germany, 2016.
5. Kondo, Y. Fatigue under variable amplitude loading. In *Comprehensive Structural Integrity*; Ritchie, B.L., Murakami, Y., Eds.; Elsevier: Amsterdam, The Netherlands, 2003.
6. Tilly, G.P. Fatigue of Steel Reinforcement Bars in Concrete: A Review. *Fatigue Fract. Eng. Mater. Struct.* **1979**, *2*, 251–268. [[CrossRef](#)]
7. Schijve, J. *Fatigue of Structures and Materials*; Springer: Berlin/Heidelberg, Germany, 2009.
8. British Standards Institution. *Guide to Fatigue Design and Assessment of Steel Products. BS 7608:2014*; British Standards Institution: London, UK, 2014.
9. Lee, S.B. Stress analysis and design for a structural fatigue testing machine. *KSME J.* **1991**, *5*, 115–124. [[CrossRef](#)]
10. Vincent, M.K.; Varghese, V.; Sukumaran, S. Fabrication and Analysis of Fatigue Testing Machine. *Int. J. Eng. Sci.* **2016**, *5*, 2319–1813.
11. Bhatkar, O.P.; Mhatre, S.Y.; Pilankar, A.S.; Desai, V.S.; Katlikar, M.J. Design and fabrication of combined fatigue testing machine. *Int. Adv. Res. J. Sci. Eng. Technol.* **2017**, *4*. [[CrossRef](#)]
12. Pach, E.; Korin, I.; Ip Na, J.P.; Pach, C.E. Simple fatigue testing machine for fiber-reinforced polymer composite. *Exp. Tech.* **2012**, *36*, 76–82. [[CrossRef](#)]
13. Cooper Technology . Large Hydraulic Four Point Bending Machine. Available online: <https://cooper.co.uk/shop/asphalt-testing/large-hydraulic-four-point-bending-machine/> (accessed on 27 June 2018).
14. Instron . Dynamic and Fatigue Testing Systems. Available online: <http://www.instron.us/en-us/products/testing-systems/dynamic-and-fatigue-systems> (accessed on 27 June 2018).
15. Considine, D.M.; Considine, G.D. *Standard Handbook of Industrial Automation*; Springer: Berlin, Germany, 1986.
16. Lynwander, P. *Gear Drive Systems: Design and Application*; CRC Press: Boca Raton, FL, USA, 1983.
17. International Organization for Standardization. *Welding—Fusion-Welded Joints in Steel, Nickel, Titanium and Their Alloys (Beam Welding Excluded)—Quality Levels for Imperfections. BS EN ISO 5817:2014*; ISO: Geneva, Switzerland, 2014.
18. Kucharczyk, P.; Rizos, A.; Münstermann, S.; Bleck, W. Estimation of the endurance fatigue limit for structural steel in load increasing tests at low temperature. *Fatigue Fract. Eng. Mater. Struct.* **2012**, *35*, 628–637. [[CrossRef](#)]
19. European Committee for Standardization. *EN 1993-1-9: Eurocode 3: Design of Steel Structures—Part 1-9: Fatigue*; European Committee for Standardization: Brussels, Belgium, 2005.
20. Rubert, T.; Perry, M.; Fusiek, G.; McAlorum, J.; Niewczas, P.; Brotherston, A.; McCallum, D. Field demonstration of real-time wind turbine foundation strain monitoring. *Sensors* **2017**, *18*, 97.
21. Fusiek, G.; Rubert, T.; Niewczas, P.; McAlorum, J.; Perry, M. Preliminary characterization of metal-packaged fiber Bragg gratings under fatigue loading. In Proceedings of the IEEE International Instrumentation and Measurement Technology Conference (I2MTC), Turin, Italy, 22–25 May 2017 .



© 2018 by the authors. Licensee MDPI, Basel, Switzerland. This article is an open access article distributed under the terms and conditions of the Creative Commons Attribution (CC BY) license (<http://creativecommons.org/licenses/by/4.0/>).